CONCRETE LIBRARY OF JSCE NO. 27, JUNE 1996

ANALYSIS OF THE DRYING SHRINKAGE BEHAVIOR OF CONCRETE USING A MICROMECHANICAL MODEL BASED ON THE MICROPORE STRUCTURE OF CONCRETE

Translation from proceedings of the JSCE,
No.514/V-27, May 1995 and No.520/V-28, August 1995

Takumi SHIMOMURA

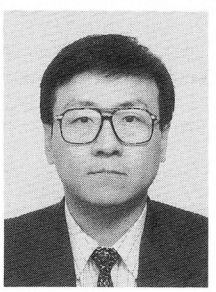

Koichi MAEKAWA

A micromechanical model for the moisture diffusion within concrete and the associated shrinkage of concrete is presented in this paper. The model is based on the micropore structure of the concrete and the thermodynamic behavior of the water in the pores. Drying shrinkage behavior, both time-dependent moisture loss and volumetric change, of mortar and concrete specimens are analyzed under various conditions. The suitability and applicability of the proposed model are discussed based on the results.

Keywords : drying shrinkage, moisture transport, pore size distribution, micromechanism

---

Takumi Shimomura is an Associate Professor in the Department of Civil and Environmental Engineering at Nagaoka University of Technology, Niigata, Japan. He obtained his Doctor of Engineering degree from the University of Tokyo in 1993. His research interests include the mechanism of creep and the shrinkage of concrete, and the transport phenomena in concrete. He is a member of the JSCE, the JCI and the RILEM.

Koichi Maekawa is a Professor in the Department of Civil Engineering at the University of Tokyo. He has a doctorate degree in engineering. His research interests include the nonlinear analysis of dynamic behavior of concrete structures, and the numerical simulation of every time-dependent behavior of concrete. He is a member of the JSCE and the JCI.

---

1. INTRODUCTION

Since concrete is originally a porous material, it always contains some water within its pores in a normal environment. According to change in humidity or direct contact with water, the moisture content of concrete changes, and there is a corresponding volumetric change in the concrete. In such a volumetric change, shrinkage associated with the drying has been most significant from the viewpoint of engineering. Drying shrinkage of concrete often reduces the durability and other functionality of concrete structures, directly or indirectly, and sometimes very seriously causes cracking, deformation, and structural stress. Furthermore, drying shrinkage of concrete can occur in any type of general concrete structure. Therefore, in order to design rationally to control the functionality of concrete structures, it is necessary to predict adequately the drying shrinkage process of structures under given conditions. The objective of this study is to develop a prediction method for the drying shrinkage of concrete structures.

General numerical methods such as FEM have been already established, and high performance computers have also become easily available. Hence, the major problem in developing an accurate and applicable prediction method for structural behavior, including drying shrinkage, is that the model used should adequately represent the characteristics of actual materials. In order that, model must be good on the one hand, and material should be reliable on the other. In the case of concrete, this problem is considerable. Properties of concrete in real structures have often been unreliable due to defects caused by substandard construction work and lack of homogeneity in the material caused by bleeding. In particular, construction work related defects cannot be easily evaluated due to human error[1]. This problem, however, has almost been solved by the High-Performance Concrete developed by the University of Tokyo in 1988 and now being universally applied[2]. This concrete can be applied uniformly in any structural area without being vibrated. The development of the High-Performance Concrete has made it possible to evaluate rationally the durability of concrete structures through numerical simulation[3].

In consideration of the above, the authors carried out this study in order to develop a prediction method of drying shrinkage of concrete meeting the following requirements :
(1) The effects of concrete materials, mix proportions and curing conditions on drying shrinkage to be considered in terms of differences in pore structures.
(2) The shape and size of structures to be considered without theoretical limitations. Variations in boundary and environmental conditions, such as temperature and humidity, to be considered.
(3) Prediction not only of the mean value of strain, stress and moisture content in concrete member, but also their distribution and time-dependent variation.
(4) Input data for computation to be easily and logically determined.

In order to satisfy these requirements, the authors developed a micromechanical drying shrinkage model. In this paper, the pore structure of concrete and microscopic phenomena in pores are formulated according to simplified mechanical and thermodynamic assumptions. Drying shrinkage processes of finite concrete specimens under various conditions were analyzed according to the proposed model. Suitability and applicability of the model were discussed based on the results.

2. BASIC CONCEPT OF THE PROPOSED METHOD

The outline of the proposed prediction method for drying shrinkage of concrete is shown schematically in **Fig.1**. The basic concept of this method is to synthesize mathematical expressions of microscopic phenomena within concrete related to drying shrinkage.

The pore structure of concrete, where microscopic phenomena take place, is modelled by the distribution function of pore size. Microscopic phenomena within concrete; thermodynamic equilibrium of vapor and liquid water, their transportation, and deformation of pore structure, are formulated according to assumptions about their mechanisms. Variation in the properties of concrete due to differences in materials, mix proportions and curing conditions, can be expressed in terms of pore size distributions differences.

On the basis of the pore structural model and micromechanical assumptions, characteristics of concrete concerning drying shrinkage can be evaluated. These are isotherm characteristics, moisture diffusivity, and volumetric change due to moisture loss. In this study, they are called characteristics of concrete at the material level.

By using these characteristics of concrete at the material level, moisture transport process and time-dependent deformation of finite-sized concrete structures, under given initial and boundary conditions are computed numerically. Structural conditions (shape and size of structures and mechanical boundary conditions) and environmental conditions (temperature and humidity) are naturally taken into account at this stage. After computation, drying shrinkage behavior of structural levels, the final output of this system, can be evaluated. In the proposed method, general computational methods such as FEM can be theoretically applied to moisture transport analysis and stress analysis.

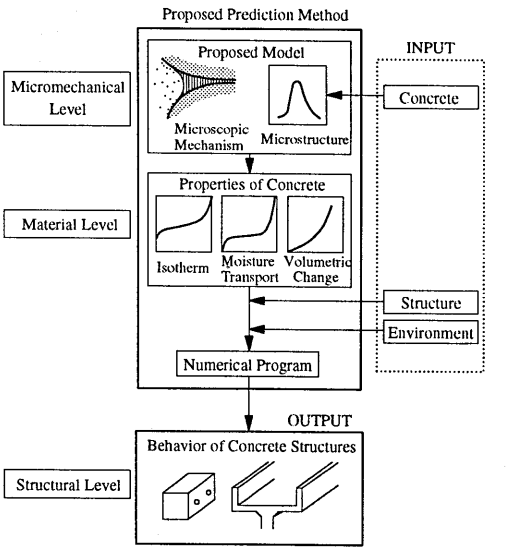

Fig.1 Outline of the proposed method

Simple empirical equations have been used for estimation of the shrinkage of concrete[4]. Though they are easy to use, they are not suitable for minute prediction involving structural detail and time-dependent variation in environmental conditions, nor for evaluation of stress distribution within structures.

Prediction methods, based on numerical simulation, have been applied to drying shrinkage and related problems[5]-[9]. In most cases, however, material models originate from macroscopic material characteristics, defined here as belonging to the material level. Concrete properties depending on mix proportions, concrete age, etc., must therefore be determined empirically. Macroscopic material characteristics cannot be quantitatively related to the micromechanism within concrete in such methods.

It has been a fundamental research topic, in the field of cement and concrete engineering, to clarify the micromechanisms of drying shrinkage and other related phenomena of concrete. Many investigations have been and are being done on this subject[10]-[14]. It seems rare in this field, however, that fundamental research is directly and effectively applied into the practical prediction of the drying shrinkage of concrete structures.

This study aims to simulate the drying shrinkage behavior of concrete at structural level, on the basis of mathematical descriptions of microscopic phenomena within concrete. This concept distinguishes this study from most previous studies dealing with drying shrinkage and related problems. Pore-structural models and micromechanical models used in the proposed system are formulated on the basis of simple mechanical and thermodynamical assumptions, in order to construct a whole system under an unified concept. This study is not characterized by the assumptions but by the methodology itself, from which the proposed system was constructed.

3. MODELLING OF PORE STRUCTURE OF CONCRETE BY THE DENSITY DISTRIBUTION FUNCTION OF PORE SIZE

The pore structural model of concrete plays a major role in the proposed system and characterizes it. There are many different kinds of pores within actual concrete, with various sizes,

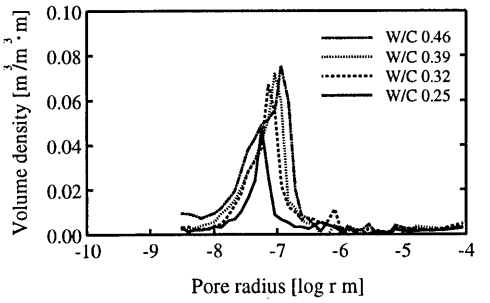

Fig.2 Examples of measured pore size distribution of mortar

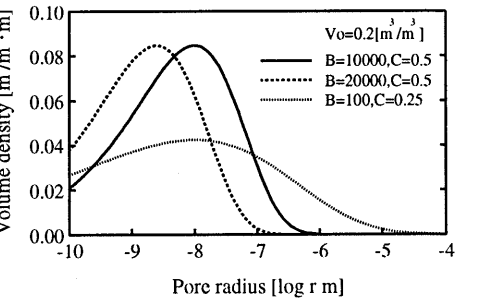

Fig.3 Modified pore size distribution

configurations, linkage structures and types of origination[15][16]. It is necessary to model all kinds of pores precisely in order to predict accurately complicated aspects of the drying shrinkage of concrete. However, precise models cannot be used easily in practical computation because of their complicated formulae. The pore structural model is required both to express important behaviors of pores in the drying shrinkage problem and also to have simple formulae suitable for computation.

One of the most important functions of the pore structure of concrete in regard to drying shrinkage is considered to be the development of the capillary force on water in fine pores due to surface tension of liquid water, or the cohesion and adhesion of water molecules, to take a more microscopic viewpoint[17]. Since this effect must be closely concerned with both moisture transport within concrete, and volumetric change in concrete due to drying and wetting[18], the pore structural model in this study was formulated so that it can suitably represent it.

One-half of the distance between solid porous wall is defined as pore radius r [m]. Pore radius r cannot take a negative value in view of its physical existence. Then, we consider the unit volume of concrete which has pore structure consisting of various radii of pores. The accumulated pore volume whose radius is not greater than r can be regarded as the function of r. This function is noted as $V_{(r)}$ [m^3/m^3]. Here, we assume that the function $V_{(r)}$ is continuous and differentiable. By differentiating $V_{(r)}$ with respect to r, we obtain the function that represents the relation between pore radius r and pore volume density whose radius is r. This function is defined as the distribution function of pore size and noted as $dV_{(r)}/dr$ [$m^3/m^3 \cdot m$].

Examples of measured pore size distributions of mortar specimens of different water-cement ratios are shown in **Fig.2**, where the relations between pore radius and pore volume density are indicated. They were obtained by means of a mercury injection method and based on several mechanical assumptions. It is evident in **Fig.2** that pore size distribution has one remarkable peak around 10^{-7} [m] of radius and that the peak varies with the water-cement ratio.

In order to represent these basic characteristics observed in measured pore size distributions, and to render them convenient for computation, the following function was taken as the density distribution function of pore size in this study[19][20].

$$\frac{dV_{(r)}}{dr} = V_O BCr^{C-1}\exp(-Br^C) \tag{1}$$

Equation (1) was determined by assuming that the accumulated pore size distribution $V_{(r)}$ followed a simple formula.

$$V_{(r)} = V_O\{1-\exp(-Br^C)\} \tag{2}$$

where, V_O : total volume of pores per unit concrete volume [m^3/m^3],
B, C : parameters which determine configuration of pore size distribution.

Examples of pore size distribution represented by **Eq.(1)** are shown in **Fig.3**. Combinations of parameters B and C determine the sharpness and the peak of pore size distributions. In mathematical representations of this model, types of pores could not be distinguished. However, the pores modelled here are intended to correspond mainly with the pores that had been filled with water in a fresh concrete state[15][16].

4. MODELLING OF MICROSCOPIC PHENOMENA WITHIN CONCRETE

4.1 Static behavior of water in pore structures

a) Basic assumptions concerning materials in pores

The following basic assumptions are made concerning materials in pores within concrete and those exposed to the atmosphere.
(1) The phases of materials in pores are gas and liquid.
(2) The gas phase is an ideal gas mixture composed of vapor and dry air.
(3) Component of liquid phase is incompressible pure water having viscosity and surface tension.
Concerning the third assumption, it is also assumed that the behavior of all liquid water in pores is governed by the same mechanism, wherever it exists. This is a simplistic assumption regarding the behavior of water. Generally, surface tension and viscosity of water is defined only at the level where water can be treated as a continuous liquid. In order to accurately represent the behavior of water at the molecular level, such as the physical and chemical adsorption of water on solid surface, other theories should be applied[21]. Furthermore, the behavior of water in the pores of hardened cement paste might actually be different from that of pure liquid water because of, for example, the solution of ions[22]. However, since it seems very difficult to take these factors into account at this stage, the assumption given above is made in this study.

b) Mechanical equilibrium of gas and liquid phases

Liquid water in fine pores develops a curved interface with gas, because of the cohesion and adhesion of water molecules. The pressures of gas and liquid phases at their interface are not equal. This fact can be hydrostatically explained from the viewpoint of the surface tension of liquid water. The relation between the pressures of the gas and liquid phases is described by the Laplace's equation as follows[23].

$$p_G - p_L = \frac{2\gamma}{r_s} \tag{3}$$

where, p_G : pressure of gas phase [Pa],
p_L : pressure of liquid phase [Pa],
γ : surface tension of liquid water [N/m],
r_s : curvature of the interface (= radius of capillary) [m].
Note that **Eq.(3)** can be derived when the contact angle between liquid water and the solid wall is zero, and the interface is a part of an ideal spherical surface.

In this study, the relation in **Eq.(3)** is assumed to be applicable to water in concrete pores. It is assumed, in other words, that the pressure gap between the gas and liquid phases in the concrete pores can be represented by **Eq.(3)**, using the pore radius r_s where the interface of the gas and the liquid phases is developed.

c) Thermodynamical equilibrium of vapor and liquid water

Among the thermodynamical behaviors of vapor and liquid water in pores in concrete, static evaporation and condensation are emphasized in this study. Adsorption and adhesional wetting of water molecule on solid wall were not considered.

The equilibrated partial pressure of vapor in fine pores varies with the curvature of the interface between the gas and liquid phases[17][23]. When the interface is a part of an ideal spherical surface, this relation can be described by the Kelvin's equation as below[23]:

$$\ln\frac{p_V}{p_{VO}} = -\frac{2\gamma M_W}{RT\rho_L}\frac{1}{r_S} \tag{4}$$

where, p_V : partial pressure of vapor [Pa],
p_{VO} : saturated partial pressure of vapor [Pa],
M_W : molecular mass of water [kg/mol],
R : gas constant [J/mol · K],
T : absolute temperature [K],
ρ_L : density of liquid water [kg/m^3].

It is assumed that **Eq.(4)** is applicable in evaluating the partial pressure of vapor in concrete pores. It is also assumed that the equilibrated state under a given relative humidity p_V/p_{VO} is uniquely limited as the state when pores whose radii are smaller than r_S in **Eq.(4)** are filled with liquid water. The transition process from one state to another is assumed to be completely reversible. The equilibrated state of vapor and liquid water in the pore structure, as expressed under these assumptions, is schematically shown in **Fig.4**.

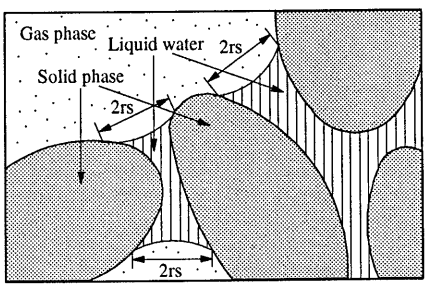

Fig.4 Vapor and liquid water in pores

The following assumption of local equilibrium[24] is also made. Each very small portion which has finite volume in the concrete, is always in an equilibrated state even when there are macroscopic gradients of properties, such as temperature, pressure and density of vapor, and when accordingly transport processes are going on. This assumption means that formulated relations among the state properties in a static process are locally applicable even in a dynamic process.

4.2 Dynamic behavior of water in pore structure

a) Mass conservation equations

To simplify the modelling, the following factors have not been taken into account in this study; the consumption of water and the development of pore structure due to hydration of cement, and the interaction between moisture and heat transport. Hence, mass conservation equations of vapor and liquid water in concrete can be expressed as follows:

$$\frac{\partial w_V}{\partial t} = -div(J_V) + v \tag{5}$$

$$\frac{\partial w_L}{\partial t} = -div(J_L) - v \tag{6}$$

where, t : time [s],
w_V : mass of vapor per unit volume [kg/m^3],
w_L : mass of liquid water per unit volume [kg/m^3],
J_V : mass flux of vapor [kg/m^2 · s],
J_L : mass flux of liquid water [kg/m^2 · s],
v : phase transition rate [kg/m^3 · s].

Phase transition rate v is defined as positive for evaporation from liquid water to vapor. If we

know mass flux J_V and J_L, we can compute moisture content at each point in time, in each portion, in a given concrete structure by discretizating **Eq.(5)** and **(6)** with respect to time and coordinate. No additional physical law is needed with regard to the phase transition rate ν because the assumption of local equilibrium implies that phase transition always takes place in any local portion, so that static equilibrium is satisfied.

b) Transport of vapor

The gas phase was assumed as an ideal gas mixture composed of vapor and dry air. Thus, the velocity of vapor with respect to the fixed coordinate can be expressed by the superposition of average velocity of the whole gas phase and the relative velocity of vapor to the whole gas phase[24].

In concrete pores, gas is forced through narrow and tortuous paths. The whole gas phase may not be easily transported within pore structure as bulk flow. However, relative movements of vapor, in other words the binary diffusion of vapor and dry air, will take place even in the pore structure of concrete, because the main mechanism of diffusion is random movement of gas molecules[25]. Hence, the mass concentration of the gas phase is assumed to be still. The binary diffusion of vapor and dry air is taken into account with regard to the transport mechanism of vapor.

The diffusion rate of vapor in the pore structures must be smaller than that in free space because the pores in concrete are not necessarily always effective for diffusion and the paths are narrow and tortuous. Mass flux of vapor in concrete is assumed as follows[25]:

$$J_V = -K_V V_G D_{VO} \, grad \, \rho_V \tag{7}$$

where, K_V : material coefficient for transport of vapor,
V_G : volume of gas phase per unit concrete volume [m^3/m^3],
D_{VO} : diffusivity for the system of vapor and dry air [m^2/s],
ρ_V : density of vapor [kg/m^3].
This formula is relevant if the gas phase has no density gradient.

Coefficient K_V is a nondimensional material factor which represents the effects of narrowness, linkage and tortuosity of the pore structures of concrete. Coefficient K_V should be less than 1 and greater than zero because it is defined as the ratio of the diffusion rate of vapor in concrete to that in free space. The volume of gas phase V_G, which is a variable dependent on the moisture state in pores, represents the space effective for diffusion. It is assumed that pores filled with gas are all effective.

c) Movement of liquid water

It is not well understood that liquid water can move within concrete when its boundary surfaces are all subjected to humid atmosphere. However, the experimentally known fact that measured moisture diffusivity in concrete increases with the increasing of water content[8][26] implies that the movement of liquid water takes place within the concrete, because the effective space for vapor diffusion must decrease as the water content increases. There must be some dominant mechanism regarding moisture movement near the saturated state. This mechanism can be assumed to be the movement of liquid water[18]. Thus, movement of liquid water is taken into account in this study.

According to the assumptions explained above, the pressure of liquid water in nonsaturated concrete is lower than that during the gas phase due to capillary tension (**Eq.(3)**). It is assumed that the gradient of this capillary tension motivates the transport of liquid water. The state of flow is assumed as a laminar flow, because the velocity might be very slow. The effects of linkage and tortuosity of pore structure are represented by a nondimensional material factor as well as vapor diffusion. The velocity of liquid water in pores whose radii are r is formulated as follows[27]:

$$v_{L(r)} = -K_L \frac{r^2}{8\mu} grad(-\frac{2\gamma}{r_s}) \quad (8)$$

where, $v_{L(r)}$: velocity of liquid water in pores whose radii are r [m/s],
K_L : material coefficient for the movement of liquid water,
μ : viscosity of liquid water [Pa · s].

Coefficient K_L represents the effects of linkage and tortuosity of pore structure on the movement of liquid water. Coefficient K_L should be less than 1 and greater than zero because it is defined as the ratio of the velocity of liquid water in concrete to that in a straight circular pipe. Both coefficients K_L and K_V actually depend on the characteristics of the pore structure of concrete. It is very difficult, however, to evaluate them directly from the pore size distribution. These coefficients are determined experimentally in this study.

Mass flux of liquid water is evaluated by coupling the assumed velocity law **Eq.(8)** and the distribution fuction of pore size. Total mass flux of liquid water is expressed mathematically as the integration of the density of mass flux of each pore where liquid water is transported. At the simplest level of assumption, all pores filled with liquid water are effective for transport. Total mass flux of liquid water can be expressed as follows:

$$J_L = \int_0^{r_s} \{\rho_L \frac{dV_{(r)}}{dr} v_{L(r)}\} dr \quad (9)$$

In reality, all pores filled with liquid water are not effective for the movement of liquid water. It is reported that the resistance to mass transportation is closely related to the quantity of pores whose sizes are greater than 10^{-7} [m][16]. This may be because of the blockage of fine pores and the water retention in pore walls. However, total mass flux of liquid water computed by **Eq.(9)** is not altered significantly even if pores smaller than 10^{-7} [m] are included in the integral range because the effect of pore size on the velocity of liquid water is considered in **Eq.(8)**. Hence, in this study, all pores filled with liquid water are assumed to be effective for the movement of liquid water as formulated in **Eq.(9)**.

4.3 Volumetric change in pore structure due to changes in moisture content

a) Stress due to capillary tension

Many theories have been proposed concerning the mechanisms of volumetric change in hardened cement paste due to changes in the moisture content[12][13][18]. As in most of previous studies, the concept of the transmitted stress between water and the solid wall of the pore structure and the deformation of structure due to this stress is considered in this study.

It has already been assumed that the pressure of liquid water in pores in nonsaturated concrete is not equivalent to that during the gas phase due to the surface tension of liquid water. The pressures of the gas and liquid phases are applied to pore walls where each phase has contact. So, we can consider that the pressure difference between the gas and liquid phases is relatively applied to pore wall. Since the pressure of the liquid phase is lower than that during the gas phase according to **Eq.(3)**, tensile stress should be applied on pore walls where contact is made during the liquid phase. It is assumed that this stress causes the shrinkage of concrete[13][28][29]. This stress, in its physical form, is regarded as capillary tension which can be defined at a macroscopic level and therefore, as discussed so far, cannot be applied directly to the molecular level. However, it is difficult at this stage to take account of more precise mechanisms and to express them quantitatively. Although a more precise model could be developed in a further study, the assumptions given above have been adopted in this study because of the simplicity of the physical image involved.

The total intensity of the tensile stress per unit concrete volume will depend on both the magnitude of the tension and the area where it is applied[18]. Accordingly, it is formulated as follows:

$$\sigma_S = A_S \frac{2\gamma}{r_S} \tag{10}$$

where, σ_S : capillary stress [Pa],
A_S : area factor.

Area factor A_S should be related to the amount of liquid water per unit concrete volume, because capillary stress is applied to pore walls where liquid water is in contact. At the simplest level of assumption, the area factor is expressed by the volume of liquid water per unit concrete volume V_L [m^3/m^3][19][29].

$$A_S = V_L \tag{11}$$

b) Deformation due to capillary stress

Capillary stress as defined here is different from usual stress in its mechanism of generation. Deformation due to capillary stress, thus, might be also different. However, since it is a deformation of hardened cement paste, deformation due to capillary stress is expected to have similar characteristics to ordinary deformation, such as elasto-plasticity, path-dependency and time-dependency[12][28][30]. In this study, a simple linear elastic relation is assumed between evaluated capillary stress and volumetric changes due to it[19]. The elastic modulus for capillary stress should accordingly include various aspects of actual deformation behavior:

$$\varepsilon_{sh} = \frac{\sigma_S}{E_S} \tag{12}$$

where, ε_{sh} : drying shrinkage strain,
E_S : elastic modulus for capillary stress [Pa].

Although capillary stress σ_S has the dimension of stress in its mathematical definition, it cannot be directly superposed on ordinary stress due to applied force. Capillary stress σ_S and elastic modulus E_S are defined only at the stage of the micromechanical model. In shrinkage stress analysis of concrete finite specimens, drying shrinkage strain ε_{sh}, as evaluated by this model, can be considered as initial strain.

5. CHARACTERISTICS OF CONCRETE AT THE MATERIAL LEVEL

5.1 Isotherm

Based on the pore structural model in chapter 3 and the micromechanical assumptions in chapter 4, the characteristics of concrete in drying shrinkage can be evaluated. Pores whose radii are smaller than r_S, determined by **Eq.(4)**, were assumed to be filled with liquid water. From the definition of the distribution function of pore size, the volume of gas phase V_G and the liquid phase V_L per unit concrete volume are respectively computed as follows **(Fig.5)**.

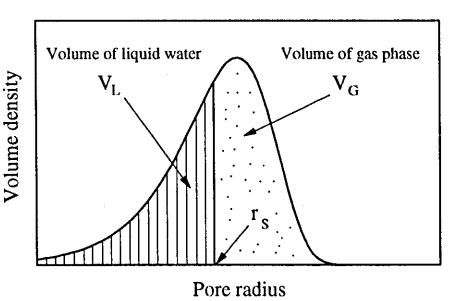

Fig.5 Volume of gas and liquid water in pore structure

$$V_G = \int_{r_s}^{\infty} \frac{dV_{(r)}}{dr} dr = V_O - V_{(r_s)} \tag{13}$$

$$V_L = \int_{0}^{r_s} \frac{dV_{(r)}}{dr} dr = V_{(r_s)} \tag{14}$$

Following the stated assumptions, it is possible that the pores whose radii are smaller than the water molecules are filled with liquid water. This condition, which never happens in reality, results from the assumption that the simple pore size distribution function with a low degree of freedom is used, and that therefore, part of the adsorbed or connected water is accounted for liquid water. This should be improved in further studies by using more realistic assumptions.

Mass of vapor w_V [kg/m^3] and liquid water w_L [kg/m^3] per unit concrete volume are expressed respectively as follows:

$$w_V = \rho_V V_G \tag{15}$$

$$w_L = \rho_L V_L \tag{16}$$

The density of the liquid water ρ_L is constant according to the assumption it is incompressible. The density and the partial pressure of the vapor are correlated with the equation for the state of ideal gas, since the gas phase is assumed to be an ideal gas mixture:

$$p_V = \rho_V \frac{RT}{M_W} \tag{17}$$

Consequently, state properties of liquid-gas two phase water in concrete, which are temperature, pressure, mass and volume, are all correlated with each other. The computed relation between relative humidity and liquid water content in concrete is shown in **Fig.6**. Water content is represented by means of the relative water content which is normalized by saturated water content. Test data presented by Okajima[31] are also plotted in **Fig.6**.

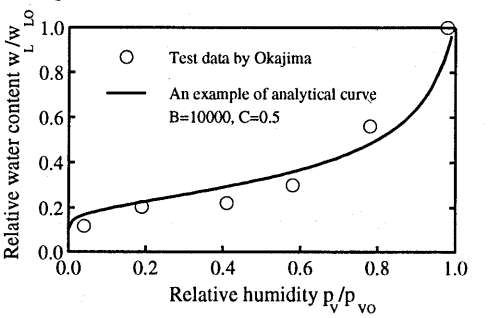

Fig.6 Relationship between relative humidity and relative water content

5.2 Moisture diffusivity

Mass conservation equations for vapor and liquid water were given as **Eq.(5)** and **Eq.(6)** respectively. Assuming that the mass change of vapor per unit concrete volume is always very small compared with that of liquid water and thus it can be neglected, we obtain a mass conservation equation for water in concrete:

$$\frac{\partial w_L}{\partial t} = -div(J_V + J_L) \tag{18}$$

Mass transportation laws for vapor and liquid water in chapter 4 were represented by means of a gradient of different variables. Using the relation among state properties, we can transform these mass transportation laws so as to be represented by means of a gradient of the mass of liquid water, which is the major variable in the moisture state in concrete.

$$J_V = -D_{V(w_L)}\, grad\, w_L \tag{19}$$

$$J_L = -D_{L(w_L)}\, grad\, w_L \tag{20}$$

where, $D_{V(wL)}$: diffusivity of vapor [m^2/s],
$D_{L(wL)}$: diffusivity of liquid water [m^2/s].
Substituting **Eq.(19)** and **Eq.(20)** into **Eq.(18)**, we obtain:

$$\frac{\partial w_L}{\partial t} = div(D_{(w_L)} grad\, w_L) \tag{21}$$

where, $D_{(wL)}$: moisture diffusivity [m^2/s].
Moisture diffusivity $D_{(wL)}$ is defined as follows;

$$D_{(w_L)} = D_{V(w_L)} + D_{L(w_L)} \tag{22}$$

Since the diffusivity of vapor $D_{V(wL)}$ and the diffusivity of liquid water $D_{L(wL)}$ are functions of the state properties of water in concrete, the total moisture diffusivity $D_{(wL)}$ is also evaluated as the function of the state properties. Consequently, we can compute moisture transport within concrete with **Eq.(21)** as the governing equation.

The dependency of the moisture diffusivity $D_{(wL)}$ on the state properties of water computed by the proposed model is shown in **Fig.7**, where the relative water content is used as the major state property. The computational curves show the tendency that the transport of liquid water develops in the higher water content state, and the dominant mechanism is substituted for the vapor diffusion with the decrease in water content. In **Fig.7**, one of the experimental curves presented by Sakata[26] is also demonstrated.

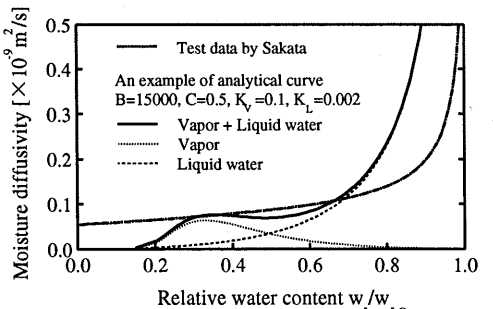

Fig.7 Relationship between water content and moisture diffusivity in concrete

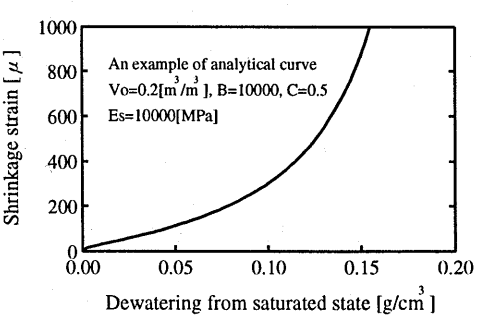

Fig.8 Relationship between dewatering and shrinkage of concrete

5.3 Volumetric change characteristics

Based on the distribution function of the pore size and the assumptions of capillary stress and deformation, we can compute the characteristics of concrete in relation to volumetric change due to drying. The relation between dewatering from a saturated state and shrinkage strain is shown in **Fig.8**.

6. BOUNDARY CONDITION

Moisture transfer through the surface exposed to the atmosphere is significant. This is the boundary condition in the drying shrinkage of concrete. In this study, this boundary condition is

treated in a similar way with heat transfer between solid and fluid[32]. It is assumed that the mass flux of water on boundary surface is evaluated by the following law:

$$J_B = \alpha_B (w_L - w_{LB}) \tag{23}$$

where, J_B : mass flux of water at boundary surface [kg/m^2 · s],
α_B : moisture transfer coefficient [m/s],
w_L : water content of concrete at the surface [kg/m^3],
w_{LB} : equilibrated water content to atmosphere [kg/m^3].

Moisture transfer coefficient α_B must be affected by the state of air flow around the concrete surface, the pore structure of concrete, and the moisture state in pores near the surface. Considering these factors, we assume the moisture transfer coefficient to be:

$$\alpha_B = \frac{D_{(w_L)}}{h} \tag{24}$$

where h is a factor, having dimension of length, that represents the state of humidity distribution in the atmosphere near the surface. In order to express the effects of the pore structure and the moisture state of concrete, moisture diffusivity within concrete is directly applied based on consideration of its similarity in a physical sense and convenience of modelling.

7. VERIFICATION

7.1 General

The proposed drying shrinkage model was verified experimentally. Since the model is based on several assumptions about the pore structure of concrete and microscopic phenomena in concrete, the acceptability of the model depends on the logic of the assumptions. Systematic shrinkage tests were carried out under various conditions. The material parameters for the model were identified from obtained experimental data by means of the inverse analysis. The applicability of the proposed model was verified by comparing the computational results with the experimental ones. The acceptability of the micromechanical assumptions are discussed, based on the relation between experimental conditions and the material parameters obtained from the inverse analysis.

7.2 Outline of the experiments

Thirty-four mortar and concrete specimens were subjected to drying under various conditions. Their drying shrinkage behavior, which were time-dependent weight and length change, were measured. Experimental conditions were varied within the following ranges.

water-powder ratio in volume	: 85～173 [%]
water-cement ratio in weight	: 25～90 [%]
volumetric ratio of aggregate (sand and gravel)	: 21～62 [%]
curing condition (testing age)	: 16 [hr] ～34 [day]
specimen size	: 4x4x16 [cm] and 10x10x40 [cm]
environmental condition	: vacuum dry and 60 [%RH]

Mix proportions of mortar and concrete are shown in **Table 1**. The conditions under which specimens were tested are shown in **Table 2**. The mix proportions were determined principally according to those of High-Performance Concrete[2]. Several kinds of powder material, including ordinary portland cement, moderate-heat portland cement, limestone powder, blast furnace slag, and fly ash, were used in small water-powder ratios. High-Performance Concrete, which was developed at the University of Tokyo, was originally designed with a low water-powder ratio to ensure self-compactability, which is the most important virtue of this concrete. Accordingly, the kind of powder material is dominant factor in considering the properties of hardened High-Performance Concrete. Compressive strength on the 28th day following standard curing conditions were 54.2 [MPa] for mix proportion MS100C, 33.0 [MPa] for MS60L740C, and 19.6 [MPa] for MS40L460C.

Table 1 Mix proportions of concrete and mortar

Name of mix proportion	V_W/V_P [vol%]	W/C,MC [%]	V_{ags} [vol%]	Unit weight [kg/m³]										
				W	C	MC	L18	L7	L4	S6	FA	S	G	Ad.
MS100C	100	33.5	62.1	172	—	513	28	—	—	—	—	828	827	8.12
MS100M	100	33.5	45.5	247	—	738	40	—	—	—	—	1191	—	11.67
MS60L740C	100	55.8	62.1	172	—	308	17	184	—	—	—	828	827	7.64
MS60L740M	100	55.8	45.5	247	—	443	24	265	—	—	—	1191	—	10.98
MS40L460C	100	83.9	62.1	172	—	205	11	—	276	—	—	828	827	7.38
MS40L460M	100	83.9	45.5	247	—	295	16	—	397	—	—	1191	—	10.62
MS60S640M	100	55.8	45.5	247	—	443	24	—	—	288	—	1191	—	11.33
OPCM	173	55.0	53.7	250	455	—	—	—	—	—	—	1407	—	1.14
S5P10	100	31.6	35.0	325	—	1030	—	—	—	—	—	917	—	10.30
S5P9	90	28.4	35.0	308	—	1084	—	—	—	—	—	917	—	10.84
S5P8	80	25.3	35.0	289	—	1144	—	—	—	—	—	917	—	11.44
S7P10	100	31.6	49.0	255	—	808	—	—	—	—	—	1284	—	8.08
S3P10	100	31.6	21.0	395	—	1252	—	—	—	—	—	550	—	12.52
G0	85	89.7	47.0	234	261	—	—	—	—	241	242	1231	—	7.44
G25	85	89.7	54.9	198	220	—	—	—	—	203	204	1045	407	6.27
G50	85	89.7	62.9	161	180	—	—	—	—	166	166	862	813	5.12

Note) V_W/V_P : volumetric ratio of water and powder materials (C, MC, L18, L7, L4, S6 and FA)
W/C,MC : water-cement (C or MC) ratio by weight
V_{ags} : volumetric ratio of sand + gravel
C : ordinary portland cement, specific gravity 3.17[g/cm³]
MC : moderate heat cement, specific gravity 3.15[g/cm³]
L18 : limestone powder,specific gravity 2.68, blane value 18000
L7 : limestone powder, specific gravity 2.67, blane value 7000
L4 : limestone powder, specific gravity 2.67, blane value 4000
S6 : blast furnace slag, specific gravity 2.91, blane value 6000
FA : fly ash, specific gravity 2.19
S : river sand, specific gravity 2.62, water absorption 1.54[%], maximum solid volume 70[%], FM 3.01
G : crushed gravel, specific gravity 2.71, water absorption 0.6[%], maximum solid volume 61[%], FM 6.85
Ad. : super plasticizer, AE admixture in OPCM

After casting and up to testing, specimens were shielded from both drying and wetting by polyethylene sheeting. The concrete age exposed to drying varied between 16 hours and 34 days. At the designated age of drying, contact tips for length measurement were attached onto the two side surfaces of the specimens with epoxy type adhesive. Then, specimens were exposed to drying under designated conditions. Time-dependent weight and length changes were measured. The shrinkage strain was zero when the drying time was zero.

Drying conditions for specimens were vacuum drying and 60 [%RH]. In the vacuum drying test, specimens were dried in a glass desiccator of 20 [*l*] capacity connected with a vacuum pump whose exhaust ability was about 50 [*l*/min][33][34]. This testing method was used because the shrinkage behavior of the specimens could be magnified and the drying condition could be easily controlled.

Table 2 Teat series

Name of specimen	Mix proportion	Size [cm]	Testing age[day]	Drying condition
MS16	MS100M	4x4x16	0.67(=16[hr])	Vacuum dry
MS2	MS100M	4x4x16	2	Vacuum dry
MS7	MS100M	4x4x16	7	Vacuum dry
MSM	MS100M	4x4x16	7	60[%RH]*
MSC	MS100C	10x10x40	7	60[%RH]*
L72	MS60L740M	4x4x16	2	Vacuum dry
L77	MS60L740M	4x4x16	7	Vacuum dry
L7M	MS60L740M	4x4x16	7	60[%RH]*
L7C	MS60L740C	10x10x40	7	60[%RH]*
L42	MS40L460M	4x4x16	2	Vacuum dry
L47	MS40L460M	4x4x16	7	Vacuum dry
L4M	MS40L460M	4x4x16	7	60[%RH]*
L4C	MS40L460C	10x10x40	7	60[%RH]*
S62	MS60S640M	4x4x16	2	Vacuum dry
S67	MS60S640M	4x4x16	7	Vacuum dry
OP2	OPCM	4x4x16	2	Vacuum dry
OP7	OPCM	4x4x16	7	Vacuum dry
S5P10	S5P10	4x4x16	2	Vacuum dry
S5P9	S5P9	4x4x16	2	Vacuum dry
S5P8	S5P8	4x4x16	2	Vacuum dry
S7P10	S7P10	4x4x16	2	Vacuum dry
S3P10	S3P10	4x4x16	2	Vacuum dry
S5P10S	S5P10	4x4x16	34	60[%RH]**
S5P10L	S5P10	10x10x40	34	60[%RH]**
G02	G0	4x4x16	2	Vacuum dry
G07	G0	4x4x16	7	Vacuum dry
G015	G0	4x4x16	15	Vacuum dry
G015N	G0	4x4x16	15	60[%RH]**
G252	G25	4x4x16	2	Vacuum dry
G257	G25	4x4x16	7	Vacuum dry
G2515	G25	4x4x16	15	Vacuum dry
G502	G50	4x4x16	2	Vacuum dry
G507	G50	4x4x16	7	Vacuum dry
G5015	G50	4x4x16	15	Vacuum dry

Note) 60[%RH]* : Temperature controlled room
60[%RH]** : Temperature controlled chamber

Testing under 60 [%RH] was carried out in either a temperature-controlled room with an air conditioner or in a temperature and humidity controlled chamber. All experimental operations including casting, curing, and drying were done at a temperature of 20 [℃]. After testing, the specimens were basically dried in an oven at a temperature of 110 [℃] for more than two days. After that, their weights were measured.

7.3 Computational method

The proposed model can be used to evaluate the characteristics of concrete for moisture transport and shrinkage. If we carry out, in terms of these characteristics, moisture transport analysis and stress analysis of a finite-sized specimen under given initial and boundary conditions, we can predict its drying shrinkage behavior numerically. General computational methods, such as FEM and FDM, can be used. A simplified method was used in this study because only prismatic specimens were used. Moisture transport process was analyzed by a two-dimensional implicit FDM. Shrinkage of specimens was computed based on the assumption of a uniform deformation in one direction. The time step and size of element in computation were determined so that stable solutions could be obtained. The outline of computational procedure is shown schematically in **Fig.9**.

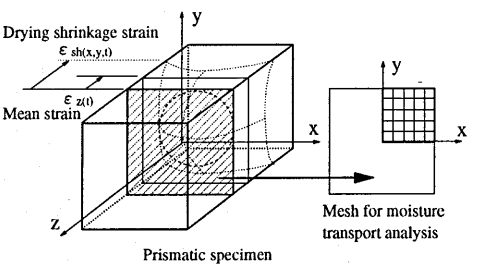

Fig.9 Analytical procedure

Table 3 Physical constants

Moleculer weight of water M_w	0.01802[kg/mol]
Gas constant R	8.31453[J/mol · K]
Density of liquid water ρ_L	1000[kg/m^3]
Saturated vapor pressure p_{vo}	2338[Pa]
Surface tension of liquid water γ	0.0727[N/m]
Diffusivity of vapor and dry air D_{vo}	0.000022[m^2/s]
Viscosity of liquid water μ	0.00098[Pa · s]

Physical constants used in this study are shown in **Table 3**. Thickness of boundary film h for moisture transport analysis was assumed to be 0.75 [mm][5][9]. For convenience of computation, the environmental condition of vacuum drying was given as 1 [%RH], which causes an approximately equal amount of evaporation with the vacuum drying.

7.4 Inverse analysis

In the proposed model, material characteristics are represented by six parameters, which are

- V_o : total volume of pores per unit concrete volume [m^3/m^3],
- B, C : parameters which determine the configuration of pore size distribution,
- K_V : parameter for vapor diffusion,
- K_L : parameter for liquid water transport,
- E_S : elastic modulus for capillary stress [Pa].

These material parameters were identified from the obtained test data of prismatic specimens following the operations of inverse analysis[3].

(1) The total volume of pores per unit concrete volume V_o is calculated from volume, initial weight, and oven-dried weight of specimens based on the assumption that the water in pores is completely evaporated by oven drying.

(2) From the test results of drying time and weight loss, equilibrated dewatering under the test conditions was determined by extrapolation (**Fig.10(a)**).

(3) The parameters B and C, which govern the configuration of pore size distribution, are determined so that the calculated relationship between relative humidity and equilibrated water content should agree with the experimentally obtained result (**Fig.10(b)**). In the series of analysis in this study, only the parameter B was determined by trial and error while the parameter C was fixed at 0.5, because combination of B and C cannot be uniquely determined from only one experimental point. The value 0.5 proved to enable reasonable width of distribution and to be suitable for numerical operations.

(4) The parameters for vapor diffusion K_V and for liquid water transport K_L are determined so that the analytical curves of drying time and weight loss of specimen would match closely with the experimental ones (**Fig.10(c)**). In this operation, the relation $K_L=K_V/50$ is assumed because these two parameters must be closely related with each other from their physical meanings.
(5) The elastic modulus for capillary stress E_S is determined so that the analytical curves of weight loss and shrinkage of specimen would match closely with the experimental ones (**Fig.10(d)**).

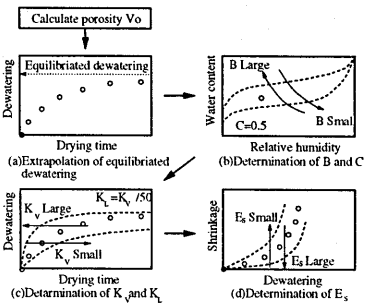

Fig.10 Determination of material parameters

These operations of inverse analysis are based on the assumption that all material parameters are constants independent of time. This assumption is not absolutely correct because material properties actually change due to the hydration of cement even in the drying process. However, because of difficulties in modelling at this stage, the assumption of constant properties was made here. The effect of this assumption on the results will be discussed.

8. RESULTS AND DISCUSSION

8.1 Applicability of the model to varied conditions

Material parameters for each specimen were obtained by the inverse analytical operations. They are all shown in **Table 4**. The drying shrinkage behavior of the specimens was computed using these parameters. The results of numerical simulation are shown together with the experimental results for several instances in this chapter. Even though material parameters were determined so that analytical results could come close to experimental ones, it is still important that the model can simulate the drying shrinkage behavior of specimens under various conditions using logically-obtained material parameters.

a) Water-cement ratio

Results for three mortar specimens with different water-cement ratios are shown in **Fig.11**. The water-cement ratios were varied by replacing cement with limestone powder. Computational results agree well with experimental ones with regard to time-dewatering (weight loss) relationship (**Fig.11(b)**), dewatering-shrinkage relationship (**Fig.11(c)**), and time-shrinkage relationship (**Fig.11(d)**).

Table 4 Material parameters

Name of specimen	V_o [m³/m³]	B	C	K_V	K_L	E_S [MPa]
MS16	0.228	8600	0.5	0.50	0.010	14000
MS2	0.204	12000	0.5	0.15	0.0030	14000
MS7	0.182	22200	0.5	0.10	0.0020	17000
MSM	0.182*	22200	0.5	0.030	0.00060	7000
MSC	0.127*	22200	0.5	0.040	0.00080	7000
L72	0.225	7600	0.5	0.25	0.0050	14000
L77	0.204	11800	0.5	0.12	0.0024	16000
L7M	0.204*	11800	0.5	0.050	0.0010	7000
L7C	0.141*	11800	0.5	0.050	0.0010	7000
L42	0.232	5000	0.5	0.30	0.0060	10000
L47	0.218	7100	0.5	0.20	0.0040	12000
L4M	0.218*	7100	0.5	0.050	0.0010	5000
L4C	0.151*	7100	0.5	0.050	0.0010	5000
S62	0.215	15400	0.5	0.18	0.0036	15000
S67	0.191	27700	0.5	0.080	0.0016	20000
OP2	0.209	9800	0.5	0.18	0.0036	13000
OP7	0.182	17000	0.5	0.12	0.0024	14000
S5P10	0.253*	15400	0.5	0.12	0.0024	14000
S5P9	0.232*	18500	0.5	0.11	0.0022	15000
S5P8	0.209*	19500	0.5	0.090	0.0018	15000
S7P10	0.198*	15400	0.5	0.12	0.0024	14000
S3P10	0.307*	15400	0.5	0.12	0.0024	14000
S5P10S	0.222*	28500	0.5	0.0075	0.00015	8000
S5P10L	0.222*	28500	0.5	0.0075	0.00015	8000
G02	0.192	9900	0.5	0.25	0.0050	12000
G07	0.162	19400	0.5	0.15	0.0030	15000
G015	0.145	24300	0.5	0.15	0.0030	20000
G015N	0.145*	24300	0.5	0.10	0.0020	8000
G252	0.166	9900	0.5	0.25	0.0050	12000
G257	0.142	19400	0.5	0.15	0.0030	15000
G2515	0.128	24300	0.5	0.15	0.0030	20000
G502	0.136	9900	0.5	0.25	0.0050	12000
G507	0.117	19400	0.5	0.15	0.0030	15000
G5015	0.106	24300	0.5	0.15	0.0030	20000

Note) * : not measured value

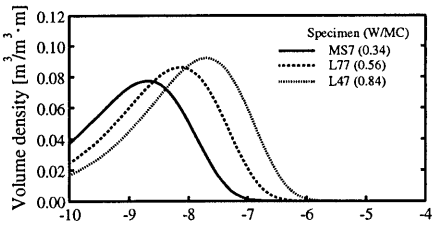

(a) Analytical pore size distribution

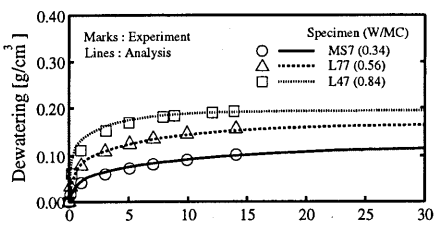

(b) Time-Dewatering relationship

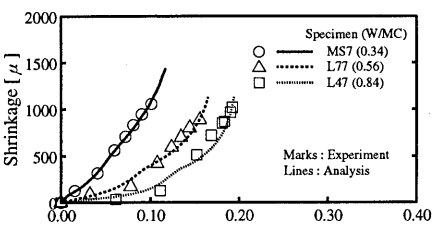

(c) Dewatering-Shrinkage relationship

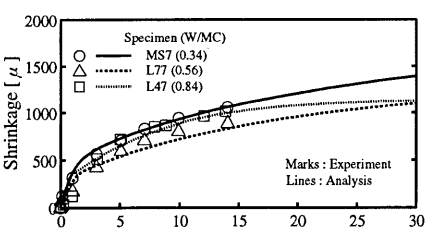

(d) Time-Shrinkage relationship

Fig.11 Experimental and analytical results of different water-cement ratio cases

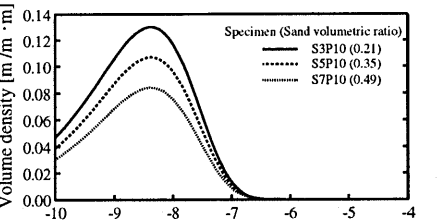

(a) Analytical pore size distribution

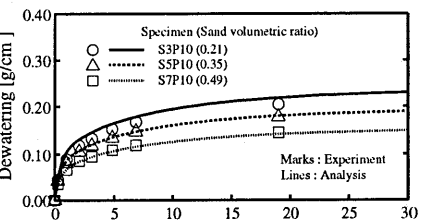

(b) Time-Dewatering relationship

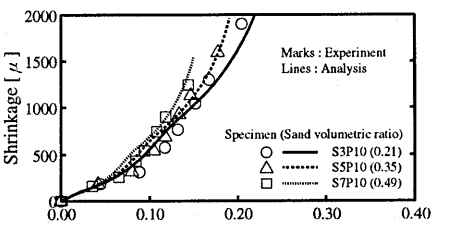

(c) Dewatering-Shrinkage relationship

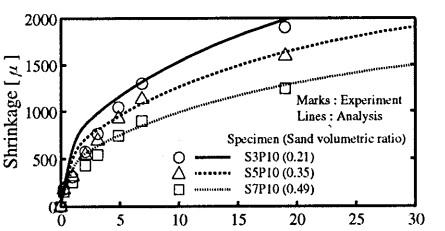

(d) Time-Shrinkage relationship

Fig.12 Experimental and analytical results of different sand volumetric ratio cases

Material parameters, identified by the inverse analysis, demonstrate that the density of pore structure (**Fig.11(a)**), the resistance to permeation of moisture, and the elastic modulus for capillary stress tend to increase with the reduction of the water-cement ratio. These tendencies are reasonable from the viewpoint of the physical understandings of these material parameters.

b) Aggregate volume

The results in cases with different aggregate volumes are shown in **Fig.12** and **Fig.13**. Figure 12 shows the results for three mortar specimens which have different sand ratios, while their mix proportions of cement paste are the same. Figure 13 shows the results for three concrete specimens which have different

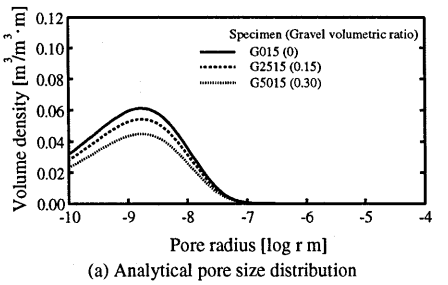

(a) Analytical pore size distribution

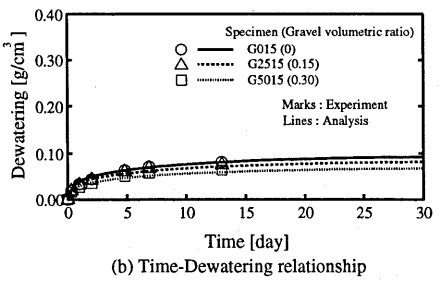

(b) Time-Dewatering relationship

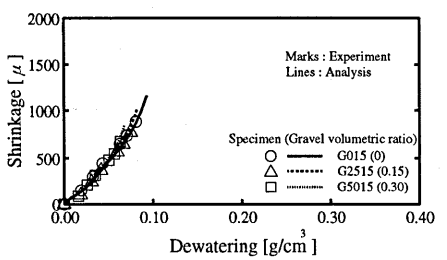

(c) Dewatering-Shrinkage relationship

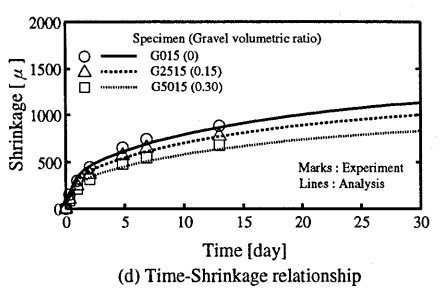

(d) Time-Shrinkage relationship

Fig.13 Experimental and analytical results of different gravel volumetric ratio cases

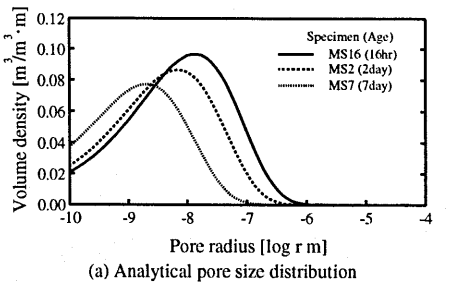

(a) Analytical pore size distribution

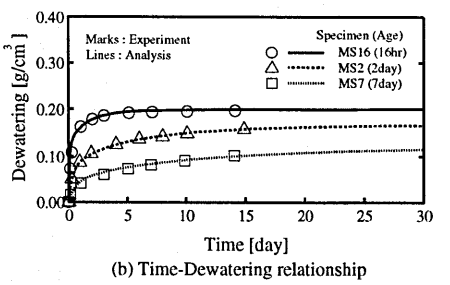

(b) Time-Dewatering relationship

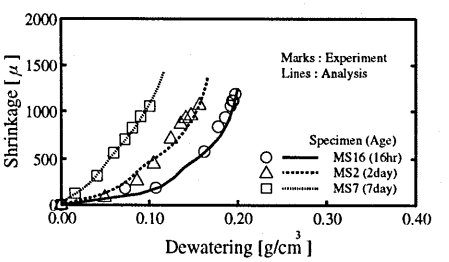

(c) Dewatering-Shrinkage relationship

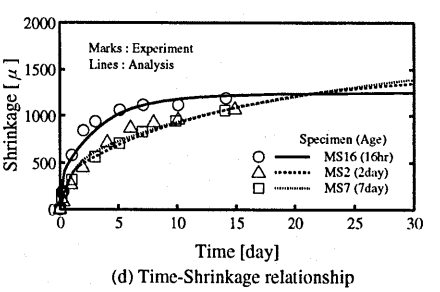

(d) Time-Shrinkage relationship

Fig.14 Experimental and analytical results of different aged specimens

gravel ratios, while their mix proportions of mortar phase are the same. Analytical results agree well with experimental results in both series. Among material parameters identified by the inverse analysis, only the total volume of pores V_o varies with the aggregate volume ratio in both series. This result implies that it is possible to approximately predict drying shrinkage characteristics of concrete of the same cement paste by considering that their pore structures in hardened cement paste are the same. However, this discussion may be limited to cases of low water-cement ratios of around 30 [%] in weight. In cases of higher water-cement ratio, pore structure of cement paste may be affected, for instance, by transition zones[15][16] which develop around the aggregate.

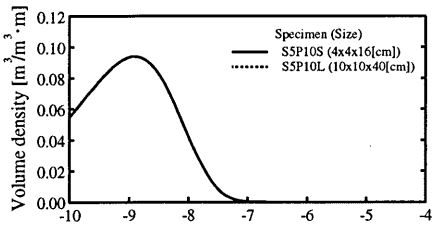

(a) Analytical pore size distribution

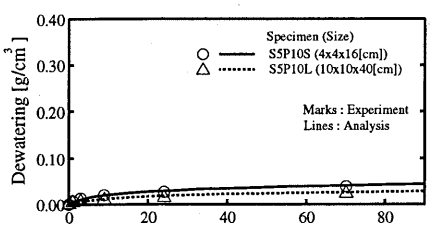

(b) Time-Dewatering relationship

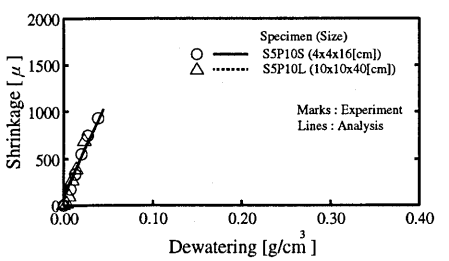

(c) Dewatering-Shrinkage relationship

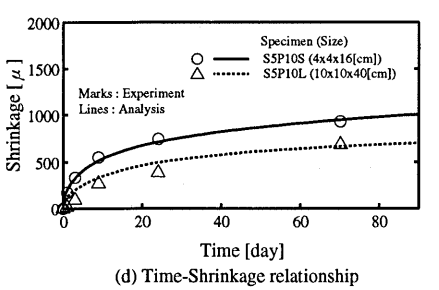

(d) Time-Shrinkage relationship

Fig.15 Experimental and analytical results of different sized specimens

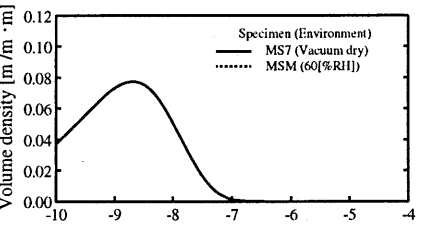

(a) Analytical pore size distribution

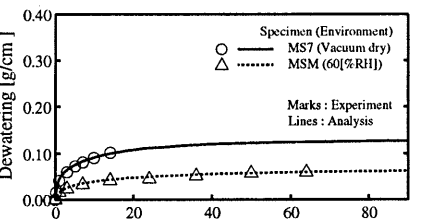

(b) Time-Dewatering relationship

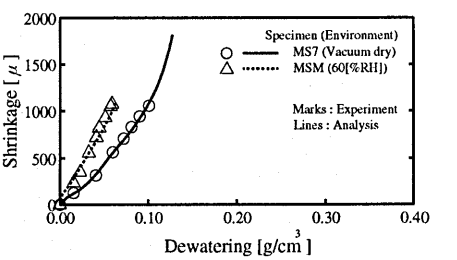

(c) Dewatering-Shrinkage relationship

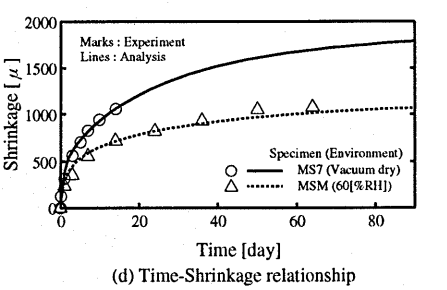

(d) Time-Shrinkage relationship

Fig.16 Experimental and analytical results of different environment cases

c) Curing condition

The results for three specimens cured under different conditions are shown in **Fig.14**. Material parameters in this serie show that a longer curing period creates a denser pore structure, higher resistance to moisture movement, and greater stiffness with regard to capillary stress.

d) Specimen size

The results for two specimens of different sizes are shown in **Fig.15**. The same values for the material parameters were used in these two cases. The proposed model represents the characteristics of the concrete itself and, therefore, can be applied theoretically to structures of any shape and size.

The results of this serie suggests the possibility of this benefit although only two examples are included here.

e) Environmental conditions

The results for two specimens under different environmental conditions, vacuum drying and 60 [%RH], are shown in **Fig.16**. Different values for material parameters (K_V, K_L, and E_S) had to be used in these cases in order for the analytical results to come close to experimental ones. The reason of this will be discussed afterwards.

8.2 Discussion concerning material parameters

It should be verified that the applicability of the proposed model to various cases was achieved using rational assumptions concerning the pore structure of concrete and the micromechanisms in pores. It is difficult, however, to verify each assumption directly by experiment, because of problems in the measurement of microscopic phenomena in concrete. In this study, assumptions concerning the model were indirectly verified by investigations of the series of material parameters obtained by the inverse analysis in **Table 4**.

a) Pore size distribution

Three material parameters concern pore size distributions.

V_o : total volume of pores per unit concrete volume [m^3/m^3],

B, C : parameters which determine configuration of pore size distribution.

The total volume of pores V_o was calculated basically from the measurement values of initial and oven-dried weights of specimens. Natural aggregates with small water absorption were used in a series of experiment. Thus, the calculated values of V_o are considered to correspond with the pore volumes filled with evaporable water.

The parameter C, which governs the sharpness of the pore size distribution, was fixed at 0.5, while the parameter B was determined from equilibrated water content. As shown in **Table 4**, the obtained values of the parameter B have scattered values from 5000 to 30000, and most of them are around 10000 to 20000. The pore radius at the peak of the pore size distribution is determined by the combination of the parameters B and C. If C is fixed at 0.5, the pore radius at the peak of the pore size distribution is 10^{-8} [m] when B=10000, and 2.5×10^{-9} [m] when B=20000 (**Fig.17**).

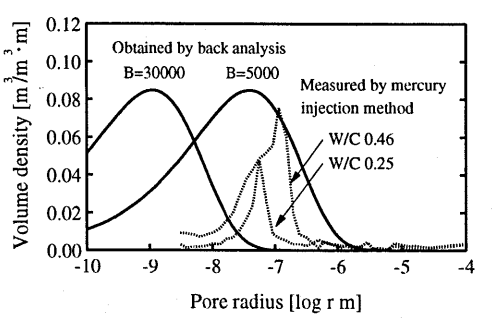

Fig.17 Comparison of analytical and measured pore size distribution

When we discuss the acceptability of obtained pore size distributions, we can make reference to the measured pore size distributions using the mercury injection method or the gas adsorption method. Examples of measured pore size distribution by the mercury injection method are also shown in **Fig.17**. Comparing the measured and the computed pore size distributions, we can regard that the pore radii at the peak of the pore size distributions obtained by analysis are 1 or 1.5 order smaller than those obtained by measurement, which are around 10^{-7} [m]. This result suggests the following possibilities.

In the mercury injection method, pore size distributions are obtained from using the relationship between the pressure during liquid phase and the radius of the interface (**Eq.(3)**). In the inverse analysis, on the other hand, they were determined from relative humidity and the volume of

condensed water using the relationship between the vapor pressure and the radius of the interface (**Eq.(4)**). Both are based on some assumptions.

There are some problems in the measurement using the mercury injection method[35]. It is difficult to measure finer pores because of the higher pressure of mercury needed for them. Some pores may be deformed or broken by the injection of the mercury. Pores into which mercury cannot be injected due to blockages are not measured. On the other hand, in the method in used this study based on the theory of capillary condensation, the volume of the finer pores may be overestimated by calculating adsorbed water as condensed if the thickness of the adsorbed water molecules is not considered[35]. Accordingly, the finer pores may not be accurately measured using the mercury injection method, while they may be overestimated by the analytical method used in this study. This hypothesis can adequately explain the tendency observed in **Fig.17**.

The pore size distribution in the proposed model is not an actual pore structure itself, but a material characteristic obtained from material behaviors and assumptions about their mechanisms. This interpretation, however, can also be applied to the mercury injection method. What are important here are the assumptions about micromechanisms. The differences between the actual and the obtained pore size distributions depend on the precision of the assumptions used.

The relationship between the experimental conditions and the obtained pore size distributions was also investigated. Figure 18 shows the relationship among the obtained parameter ***B***, the water-cement ratio, and the testing age of the specimens, which may have a major influences on the development of the pore structure of the hardened cement paste. Water-cement ratios are indicated by weight. As for the series where blast furnace slag was used, the weight of slag was calculated with that of the cement for the water-cement ratio. This arrangement resulted in an acceptable plot of the results following investigations. It may be equal to the pozzolanic effect of slag.

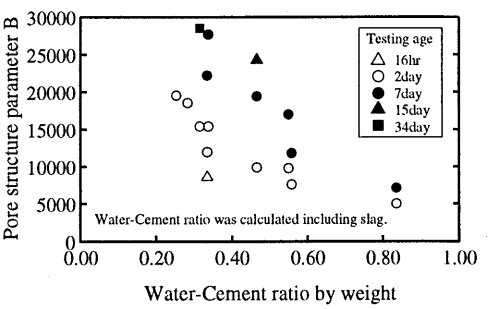

Fig.18 Relationship between water-cement ratio and pore structure parameter ***B***

In **Fig.18**, it is obvious that the parameter ***B*** takes greater value, which means a finer pore structure, with reduction in the water-cement ratio and with the increase in the curing time. This tendency is acceptable in line with general knowledge concerning the fineness of the pore structure of concrete.

Consequently, the distribution function of the pore size in the proposed model is not the actual pore size distribution itself, but can adequately represent trends of the fineness of the pore structure of concrete.

b) Coefficients for moisture transport

There are two material parameters which are concerning moisture transport within concrete.

K_V : parameter for vapor diffusion,

K_L : parameter for liquid water transport.

In the series of analyses, these two parameters were not treated independently. The relation $K_L=K_V/50$ was assumed between them, in order to make it easy to determine the material parameters by reducing the unknowns. It was verified that the computed relationship between water content, or relative humidity, and moisture diffusivity under the condition of $K_L=K_V/50$ showed similar tendencies to those in other studies[5][8][26]. This assumption means that the transport of liquid water occur in near a saturated state, and that the dominant mechanism is gradually substituted in place of vapor diffusion with the reduction of water. Considering that the analytical results of drying processes agree with the experimental results through the entire drying duration in almost all cases, we can conclude that the assumption of $K_L=K_V/50$ is acceptable.

The relationship between the experimental conditions and the obtained parameter K_V was investigated. Since it was verified in **Fig.18** that the parameter B is closely related to the experimental conditions concerning the water-cement ratio and the curing duration, the relationship between B and K_V is investigated here. The relationship between the obtained parameter B and the coefficient K_V for all cases is shown in **Fig.19**. Environmental conditions are distinguished in this figure. It is recognized that the parameter B, which represents the fineness of pore structure, has an apparent relationship with the coefficient K_V, which represents the vapor diffusivity within pore structure, and that the coefficient K_V obtained in an environment of 60 [%RH] is smaller than that obtained by the vacuum drying. As shown in **Fig.19**, the coefficient for vapor diffusion K_V takes a smaller value when the parameter B increases in value. In other words, the resistance to vapor transport within concrete increases with the greater density of pore structure. This tendency is reasonable from the viewpoint of the physical understanding of the parameters.

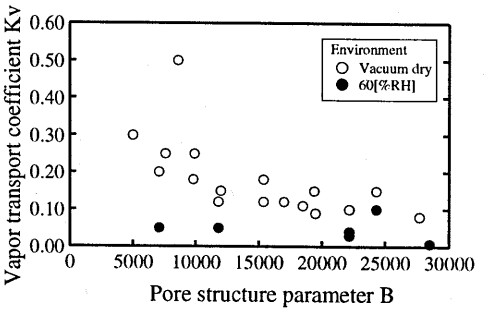

Fig.19 Relationship between pore structure parameter B and coefficient K_V

The reason why the coefficient K_V in an environment of 60 [%RH] is smaller than that obtained by the vacuum drying may be atributable to the assumptions designed to simplify the analytical operations. In the series of analyses, the change of pore structure due to hydration of cement during the test was ignored, and environmental conditions for the vacuum drying were substituted by conditions 1 [atm] and 1 [%RH]. The authors suppose that these simplifications caused the differences between K_V under 60 [%RH] and vacuum drying. Pore structure will develop further in an environment of 60 [%RH] than with the vacuum drying because the evaporation of water is slower and, therefore, the hydration of cement continues for longer. It is also demonstrated that molecular diffusivity of gas actually increases with a reduction in pressure[25]. Both of these factors may possibly contribute to the overestimation of the coefficient K_V in the vacuum drying.

It is reported that the tortuosity, having same definition with K_V in this study, is between about 0.1 and 0.7 for most porous materials[25]. The obtained coefficient K_V is around 0.1 to 0.3 for the vacuum drying and around 0.05 for 60 [%RH].

c) Elastic modulus for capillary stress

The elastic modulus for capillary stress E_S was also verified by investigating its relationship with the parameter B. The relationship between the obtained B and E_S for all cases is shown in **Fig.20**. Environmental conditions are also distinguished in this figure. It is recognized that the obtained elastic modulus E_S has a close relationship with the parameter B, and that the elastic modulus E_S in 60 [%RH] is smaller than that obtained by the vacuum drying.

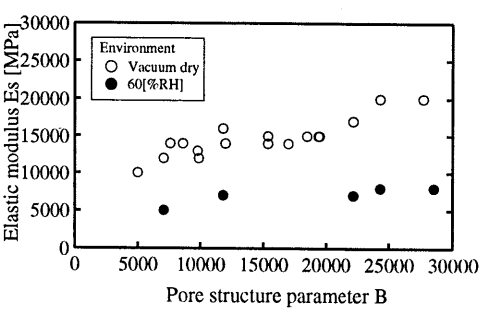

Fig.20 Relationship between pore structure parameter B and elastic modulus E_S

The relationship of B and E_S implies that the resistance to deformation increases with the greater density of the pore structure. This tendency is also reasonable from the viewpoint of the physical understandings of these parameters.

In the results, the elastic modulus obtained in 60 [%RH] were about 1/3 or 1/2 of that in the vacuum drying. The authors assume that the reason for this is the time-dependent deformation of

the pore structure due to capillary stress. As shown in **Fig.16(b)**, the rates of evaporation of water were naturally different between in 60 [%RH] and the vacuum drying. In these cases, however, the relationships between the evaporation of water and the shrinkage were also different from each other (**Fig.16(c)**). This result suggests that there may be a time-dependent component in the deformation due to capillary stress as well as in ordinary deformation due to applied stress[12][28]. Thus, if we assume a linear elastic relationship between the capillary stress and the shrinkage, the time-dependent deformation should be estimated as a reduction of the elastic modulus. The ratios of the time-dependent deformation to the observed shrinkage will be different between under 60 [%RH] and the vacuum drying because of the differences in the evaporation rate[30]. The result, that reduction ratios of elastic modulus are around 1/3 or 1/2, implies that creep coefficients are around 1 or 2. These values are close to the ordinary creep coefficient of concrete[4].

The authors assume that it is possible to describe the drying shrinkage behavior of concrete in general terms under various drying rates through considerations of the time-dependent deformation in its formulation[30][36]. A linear elastic relationship was adopted in this study between the capillary stress and the shrinkage because of its simplicity as a formula. In an actual environment, however, the effect of the time-dependent deformation will not be greater than that in the results obtained here, because the variation of humidity, and therefore the variation in evaporation rate, should be smaller than in the tests.

Changes in pore structure during the tests must have actually affected the obtained elastic modulus as well as the vapor diffusivity. This factor should make the elastic modulus in 60 [%RH] greater than that in the vacuum drying. In spite of this, the opposite result was actually obtained. The authors believe the reason for this is that the magnitude of reduction of the elastic modulus due to the time-dependent deformation was greater than its development due to the hydration of cement.

As shown in **Fig.20**, the obtained elastic modulus for capillary stress was around 10000 to 20000 [MPa] in the vacuum drying cases, approximately 1/3 or 2/3 of the ordinary values of the static elastic modulus of concrete for applied stress. This tendency was also reported in other studies where the mechanism of the drying shrinkage of concrete was investigated from the viewpoint of capillary stress[13]. This was possibly related to the assumption that the effect of capillary tension could be modelled by uniform stress in material, or by the intrinsic differences in the mechanism between the deformation due to capillary stress and that due to applied stress.

9. CONCLUSIONS

In this study, a model for the drying shrinkage of concrete based on pore structure and micromechanisms in pores was proposed. The model was verified by systematic drying shrinkage tests of mortar and concrete specimens under varying conditions. The following results can be inferred from this study.

(1) Material parameters in the model can be logically determined by the inverse analysis of the drying shrinkage behavior of prismatic specimens.

(2) The model can simulate drying shrinkage behavior, both time-dependent moisture loss and shrinkage, under varying conditions by assuming adequate material parameters.

(3) The pore size distributions obtained by the inverse analysis overestimate the volume of the finer pores due to oversimplification of the micromechanisms. It is concluded, however, that they can be used as appropriate indices of the fineness of the pore structures.

(4) The modelling of moisture transport within concrete is adequate because the material parameter for moisture transport has an acceptable relationship with the parameter for the fineness of the pore structures.

(5) Obtained elastic modulus for capillary stress has an acceptable relationship with the parameter for the fineness of the pore structures. Their magnitude is approximately 1/3 or 2/3 of the ordinary value for the static elastic modulus of concrete for applied stress. The elastic modulus for capillary stress depends on the drying rate. This fact can be explained by the hypothesis that the time-dependent component is related to the deformation due to capillary stress.

Finally, it can be concluded that the proposed drying shrinkage model can be a first step toward the prediction of the drying shrinkage behavior of concrete structures based on the consideration of micromechanisms.

ACKNOWLEDGEMENTS

The authors wish to express their sincere gratitude to Mr.K.Fukudome and Dr.Y.Edamatsu for their excellent technical help in the experiments.

REFERENCES

[1] JSCE Subcommittee on durability design for concrete structures : Proposed recommendation on durability design for concrete structures (draft), Concrete Library JSCE No.65, 1985 (In Japanese)
[2] Ozawa,K., Kunishima,K., Maekawa,K., and Okamura,H. : High Performance Concrete based on the durability design of concrete structure, Proc. of the EASEC-2, Vol.1, pp.445-450, 1989
[3] Shimomura,T., Fukudome,K., and Ozawa,K. : Evaluation of the characteristics of drying shrinkage of concrete using micro pore structural model, Proc. of the JCI Symposium on super-flowable concrete, pp.167-174, 1993 (In Japanese)
[4] Sakata,K. : Prediction of shrinkage and creep of concrete, Concrete Journal, Vol.31, No.2, pp.5-14, 1993 (In Japanese)
[5] Bazant,Z.P. and Najjar,L.J. : Nonlinear water diffusion in nonsaturated concrete, Materials and Structures, Vol.5, No.25, pp.3-20, 1972
[6] Nagamatsu,S. and Sato,Y. : Study on distribution of dewatering in concrete by nonlinear diffusion equation, Annual Report of JCA, Vol.35, pp.162-165, 1981 (In Japanese)
[7] Takiguchi,K., Hotta,H., and Koitabashi,Y. : An analysis of thermal and shrinkage stresses in concrete at early age, Transactions of AIJ, No.396, pp.118-124, 1989 (In Japanese)
[8] Akita,H., Fujiwara,T., and Ozaka,Y. : Water movement within mortar due to drying and wetting, Proc. of the JSCE, No.420/V-13, pp.61-69, 1990 (In Japanese)
[9] Numao,T., Mihashi,H., and Fukuzawa,K. : Moisture diffusion process in concrete at elevated temperatures, Transactions of AIJ, No.441, pp.1-7, 1992 (In Japanese)
[10] Kondo,M. : Relationship between state of water within hardened cement paste and drying shrinkage considering moisture diffusion, Annual Report of JCA, Vol.12, pp.136-149, 1958 (In Japanese)
[11] Powers,T.C. : Thermodynamics of volume change and creep, Materials and Structures, Vol.1, No.6, pp.487-507, 1968
[12] Tanaka,H. : Structure and properties of hardened cement paste, Porous Materials — properties and utilizations —, Chapter 13, Gihodo Shuppan, 1973 (In Japanese)
[13] Kishitani,K. and Baba,A. : Mechanisms of drying shrinkage of construction materials, Cement Concrete, No.346, pp.30-40, 1975 (In Japanese)
[14] Feldman,R.F. and Baudoin,J.J. : Concrete Science, Heydon & Son, 1981
[15] Hanehara,T. : Structures and properties of concrete, Cement Concrete, No.549, pp.31-43, 1992 (In Japanese)
[16] Hanehara,T. : Structures and properties of concrete, Cement Concrete, No.550, pp.50-63, 1992 (In Japanese)
[17] Yawata,T. : Physics of Soil, The University of Tokyo Press, 1975 (In Japanese)
[18] Young,J.F. : Physical mechanisms and their mathematical descriptions, Mathematical modeling of creep and shrinkage of concrete, Bazant,Z.P. ed., Chapter 1, John Wiley & Sons, 1988

[19] Shimomura,T., Chin,B., and Ozawa,K. : Micro pore structure and shrinkage behavior of concrete, Proc. of the 46th JSCE Annual Conference, Part 5, pp.478-479, 1991 (In Japanese)
[20] Shimomura,T. and Ozawa,K. : Analysis of water movement in concrete based on micro pore structural model, Transactions of the JCI, Vol.14, pp.115-122, 1992
[21] Arai,Y. and Iwai,Y. ed. : Physical chemistry for engineering, Chapter 9, Asakura Shoten, 1991 (In Japanese)
[22] Chaube,R.P., Shimomura,T., and Maekawa,K. : Analytical modelling for the effect of aggregates on water transport in concrete, Proc. of the JCI, Vol.15, No.1, pp.1217-1222, 1993
[23] Ono,S. : Surface Tension, Kyoritsu Shuppan, 1980 (In Japanese)
[24] Hiraoka,M. and Tanaka,M. : Transport Phenomena, Asakura Shoten, 1971 (In Japanese)
[25] Komiyama,H. : Rate Processes, Asakura Shoten, 1990 (In Japanese)
[26] Sakata,K. and Kuramoto,O. : A study on the water diffusion and shrinkage in concrete by drying, Proc. of the JSCE, No.316, pp.145-152, 1981 (In Japanese)
[27] Hino,M. : Hydraulics, Maruzen, 1983 (In Japanese)
[28] Nagataki,S. and Yonekura,A. : A study on the mechanisms of drying shrinkage and creep of concrete, Concrete Journal, Vol.20, No.12, pp.85-95, 1982 (In Japanese)
[29] Goto,T., Sakai,K., and Sato,K. : Mechanism of reducing the drying shrinkage of hardened cement by some organic additives, Cement Concrete, No.442, pp.9-15, 1983 (In Japanese)
[30] Fukudome,K. and Shimomura,T. : A model for drying shrinkage of concrete considering time-dependent deformation, Proc. of the 47th JSCE Annual Conference, Part 5, pp.944-945, 1992 (In Japanese)
[31] Okajima,T., Mizutani,A., Kawabe,S., Shimura,K., and Kachi,Y. : Sorption isotherm of concrete, Extended Abstract of the 43rd Annual Meeting of JCA, pp.350-353, 1989 (In Japanese)
[32] Yagawa,G. and Miyazaki,N. : Analysis of thermal stress, creep and heat transfer by finite element method, Science-Sha, 1985 (In Japanese)
[33] Yamanaka,K., Ozawa,K., and Kunishima,M. : Quantitative evaluation of durability of concrete structures, Proc. of the JCI, Vol.11, No.1, pp.487-492, 1989 (In Japanese)
[34] Shimomura,T., Chin,B., and Ozawa,K. : Model for prediction of drying shrinkage of concrete utilizing vacuum-dry method, Proc. of the JCI, Vol.13, No.1, pp.391-396, 1991 (In Japanese)
[35] Goto,S., Daimon,M., and Kondo,R., : Pore size distribution, Porous Materials — properties and utilizations —, Chapter 3, Gihodo Shuppan, 1973 (In Japanese)
[36] Tanaka,T. : Path-dependency in volumetric change of concrete due to drying and wetting (Graduation thesis), The University of Tokyo, 1993 (In Japanese)